Electronic Supplementary Material (ESI) for Chemical Communications

SUPPORTING INFORMATION

A Self-assembled, Metalloorganic Supramolecular Frequency Doubler

Luke Burke, Grazia Gonella, Fenton Heirtzler, Hai-Lung Dai, Stephanie Jones, Jon Zubieta and Alex Roche

Table of Contents:

S1 Synthesis

Compound **1**. A mixture of 0.25 g (0.86 mmol) of α-diketone **2**[S1] and 0.17 g (0.86 mmol) 1,2-diamino-4,5-dinitrobenzene **3**,[S2] in MeOH (ca. 3 mL) was heated 90 min. under reflux. At the conclusion of that time, volatile material was removed by rotary evaporation and the remaining material dissolved in CH_2Cl_2 (ca. 40 mL). The resulting solution was washed with water (3 x 15 mL), dried ($MgSO_4$) and concentrated in vacuum to give a dark-colored oil. Flash column chromatography (20:80-EtOAc:CH_2Cl_2; silica gel) followed by recrystallization (MeOH) gave 0.232 g (59%) of compound **1** as a beige microcrystalline solid. Mp 197.5 – 199.5 °C; Calcd for $C_{23}H_{13}N_7O_4$: C 61.20, H 2.90, N 21.72%; found: C 61.01, H 2.84, N 21.66%; ES-MS (MeOH): m/z = 452 ($[M + H]^+$, 100%).

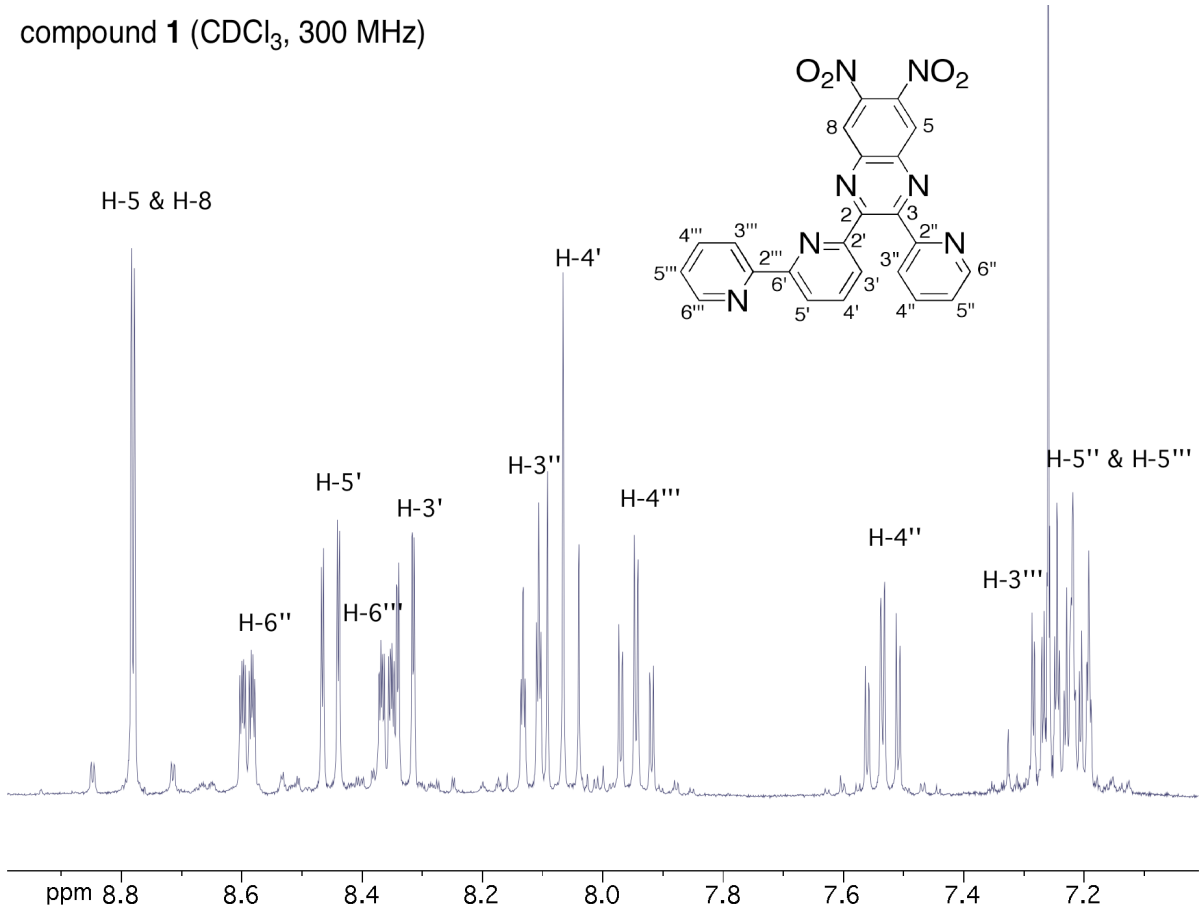

Figure S1. ^{1}H NMR spectrum of compound **1** ($CDCl_3$, 300 MHz), including assignments.

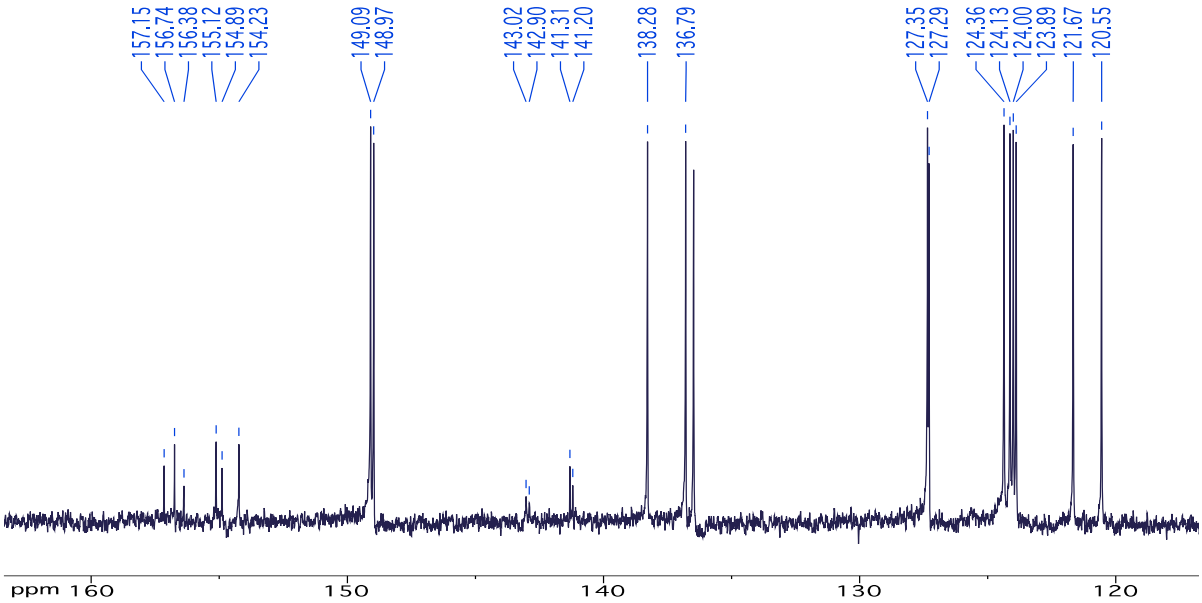

Figure S2. ^{13}C NMR spectrum ($CDCl_3$, 75 MHz) of compound **1.**

Complex [**1**$_2$Cu$_2$][PF$_6$]$_2$: A mixture of 39.9 mg (0.0888 mmol) of compound **1** and 33.3 mg (0.0893 mmol) of [Cu(CH$_3$CN)$_4$][PF$_6$] in degassed MeOH (3 mL) were heated 70 min. under reflux and N$_2$. At the conclusion of that time, volatile material was removed by rotary evaporation. The residual material was dissolved in MeCN (ca. 2 mL), filtered through Celite and recrystallised by diffusion of Et$_2$O into MeCN to give 45.3 mg (80%) of dark purple blocks. Calcd for C$_{46}$H$_{26}$Cu$_2$F$_{12}$N$_{14}$O$_8$P$_2$: C 41.86, H 1.99, N 14.86%; found: C 41.82, H 2.06, N 14.70%; ES-MS (MeOH): m/z = 514/515/516/517/518 ([**1**Cu]$^+$), 965/966/967/968 ([**1**$_2$Cu]$^+$).

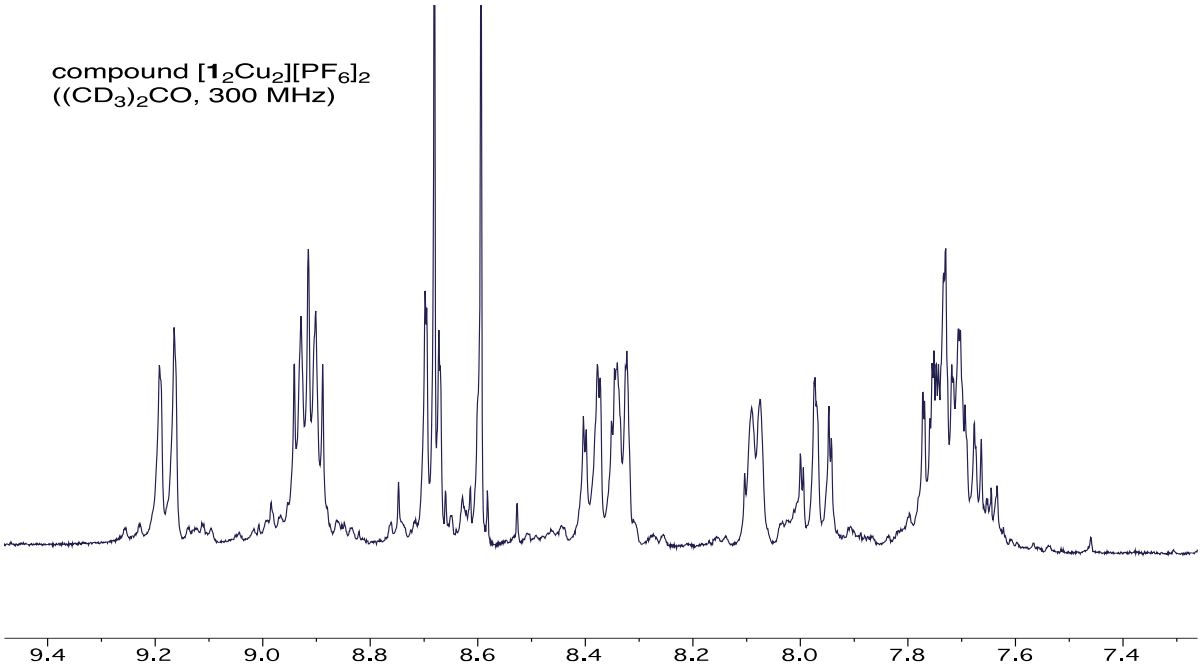

Figure S3. ^{1}H NMR spectrum ((CD$_3$)$_2$CO, 300 MHz) of [**1**$_2$Cu$_2$][PF$_6$]$_2$.

S2 Characterization

S2.1 UV-vis Spectrum

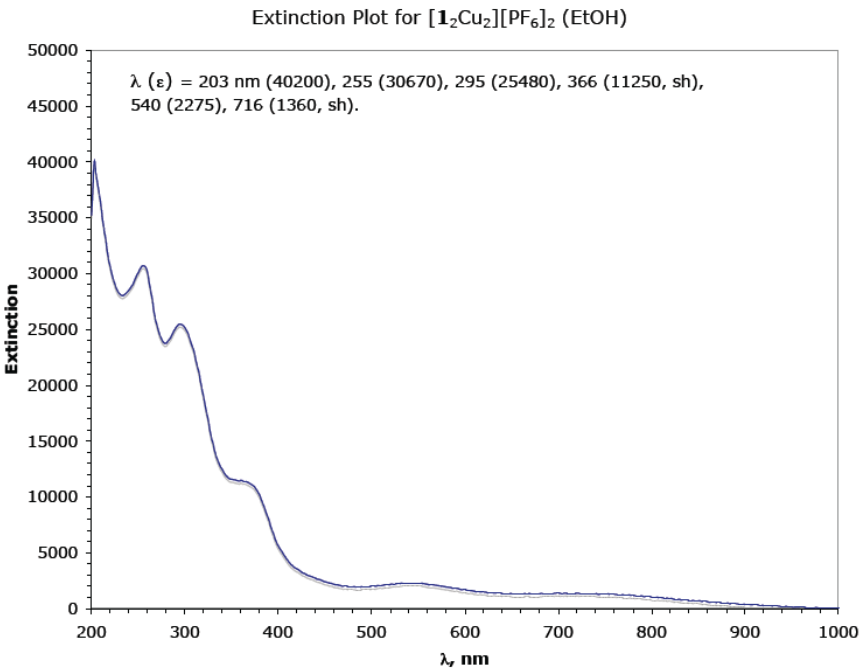

Figure S4. Electronic spectrum of $[\mathbf{1}_2Cu_2][PF_6]_2$ in absolute ethanol. Extinction in $mol^{-1}dm^3cm^{-1}$.

S2.2 X-Ray Crystal Structure Determination: General Crystallographic Details

Data were collected on a Bruker Apex II CCD Diffractometer operating at 90(2) K with Mo-Kα radiation (λ= 0.71073 Å). The unit cell contains 2 acetonitrile molecules which have been treated as a diffuse contribution to the overall scattering without specific atom positions by SQUEEZE/PLATON in addition to the 3 acetonitrile molecules found in the electron density map. This had the effect of markedly improving the agreement indices in all cases. Crystal data: $C_{46}H_{26}Cu_2F_{12}N_{19}O_8P_2$, M = 1525.10; blue needle, 0.20 x 0.14 x 0.08 mm^3, triclinic, space group P-1 (No. 2), a = 9.438(2), b = 15.912(3), c = 20.940(3) Å, V = 2939.5(9) $Å^3$, Z = 2, Dc = 1.723 g cm^{-3}, F_{000} = 1540, 29016 reflections collected, 14004 unique (Rint = 0.0617). Final GooF = 0.947, R1 = 0.0672, wR2 = 0.1573, R indices based on 7628 reflections with I > 2σ(I) (refinement on F^2).

S3. HRS Experiments

S3.1 HRS Setup

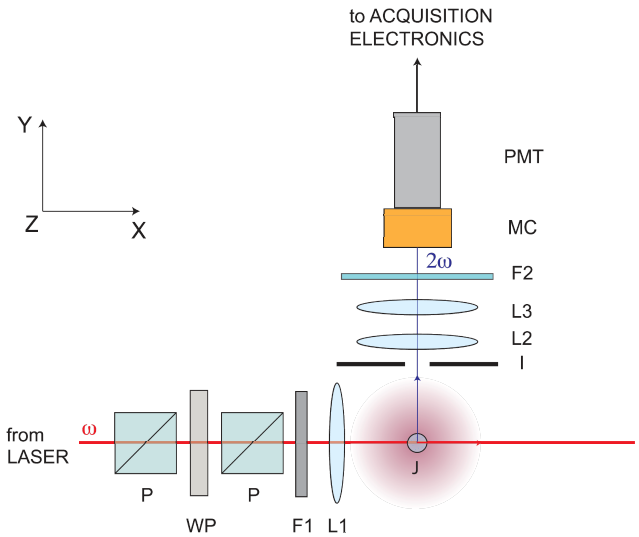

Figure S5. The HRS experimental setup. P: polarizer, WP: half-wave plate, F1: long-pass filter, L1, L2, L3: lenses, J: liquid jet, I: iris, F2: band-pass filter, MC: monochromator, PMT: photomultiplier tube.

HRS measurements are performed by focusing the output of a Ti:Sapphire laser (Coherent, Micra V oscillator) at 800 nm (pulse duration 130 fs, 78 MHz repetition rate, average power 200 mW) onto a liquid jet produced in a micropump-driven flow system. The liquid jet, already used in the past in SHG experiments,[S3-S5] is used for the first time in a HRS experiment: this setup avoids any effects that might be introduced by the presence of the cell windows. The polarization of the pump laser was set to vertical by means of a half-wave plate and polarizing cube beamsplitters and was filtered with a long-pass filter (Schott RG695) to remove any higher harmonic components that may be present in the beam. The detection is at a 90°-angle with respect to the fundamental propagation direction. An iris is used to set the detection angle resolution. The light is then collected and collimated by a system of lenses and passed through a band pass filter (Schott BG39, 340 nm - 600 nm) that blocks the fundamental beam, and is directed into a monochromator (Princeton Instrument, Acton SP2300) for spectral analysis and detected by a Photomultiplier tube (PMT) (R1527 Hamamatsu). No analyzer is present in the detection system so that the total intensity at 2ω is detected. Finally, the PMT output is amplified by a fast preamplifier (350 MHz, Stanford Research) and analyzed by a photon counting system (Stanford Research SR400) which is coupled to a microcomputer. A schematic view of this setup is presented in Fig. S5.

S3.2 HRS Theory

HRS is an incoherent type of scattering, as fluorescence, and the observed signal, at frequency twice that of the fundamental, generated from a random distribution of molecules can be

expressed by Eq. 1. When the solute absorbs at the second harmonic frequency (resonant HRS at 2ω) then the term $10^{\varepsilon(2\omega)N_C l}$ is added to the expression in Eq. 1,[S6] where $\varepsilon(2\omega)$ is the molar extinction coefficient and l the optical path length. In the present case such resonance is apparently too weak to be noticed at the concentration used in the experiments. The relation between $\langle\beta^2_{HRS}\rangle$, defined in the laboratory frame, and the molecular hyperpolarizability tensor β_{ijk}, defined in the molecular frame, depends upon the experimental configuration as well as the polarization of fundamental and second-harmonic waves[S7] (for more details see Section S4). When the fundamental is vertically polarized and the second harmonic signal is detected at a 90°-angle without selecting its polarization then, $\langle\beta^2_{HRS}\rangle = \langle\beta^2_{ZZZ}\rangle + \langle\beta^2_{XZZ}\rangle$ following the convention in Fig. S5.

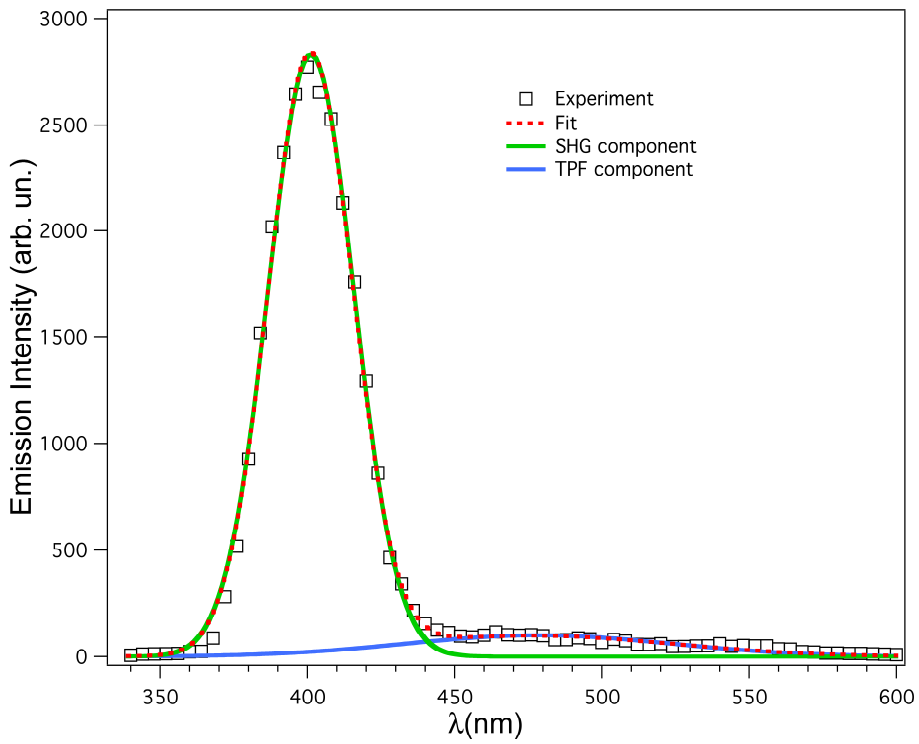

Figure S6. Experimental emission intensity (black squares). Nonlinear least square fit with two squared Gaussian functions (red dotted line): one for HRS (continuous green line) and TPF(continuous blue line).

S3.3 HRS Data Treatment and Fit

Since both HRS and two-photon fluorescence (TPF) are second-order processes and both are incoherent they show the same dependence on the fundamental intensity ($\propto I^2(\omega)$) and the solute concentration ($\propto N_C$) so extra care must be paid not to overestimate the HRS response. We chose to resolve these two contributions spectroscopically:[S7] as shown in the inset of Fig. 1, and blown up in Fig. S6, the spectrum, at high $[\mathbf{1}_2Cu_2][PF_6]_2$ concentration, can be nicely fit by a narrow peak centered at 400 nm, attributed to actual HRS and showing a FWHM consistent with that of the laser output, and a broader and much less intense peak centered at 480 nm, attributed to TPF. No other contributions to the emission are present in the emission, other than the broad TPF peak, as suggested by the 0 intensity of the background at the extreme wavelengths of the spectrum. From the fit using two squared Gaussian functions the contribution of TPF to the total

signal measured at 400 nm turns out to be less than 1%, lower than the error in our measurements: since both HRS and TPF intensities are linearly proportional to N_C, this ratio remains constant in dilution experiments and we can disregard spurious TPF contributions to the HRS signal measured at this wavelength.

The data reported in Fig. 1 are the result of several dilution experiments. For each experiments $I_0(2\omega)$, without jet, was recorded and subtracted from $I(2\omega)$, with jet. The data in Fig. 1 are the result after such subtraction and after normalization to $I^2(\omega)$. Experiments at higher concentrations were not possible because of the limited solubility of [**1**$_2$Cu$_2$][PF$_6$]$_2$ in MeOH.

By using the internal reference method,[S7-S10] $\langle\beta^2_{HRS}\rangle_C$ can be obtained by performing experiments as a function of the solute concentration, N_C as reported in Fig. 1, once the solvent $\langle\beta^2_{HRS}\rangle_S$ is known. The data can then be fit to a line: $y = mx + q$ where x and y are the abscissa and ordinate as in Fig. 1: where $m = G\langle\beta^2_{HRS}\rangle_C$ and $q = GN_S\langle\beta^2_{HRS}\rangle_S$.

S4 Computational Details

In our previous computational investigation[S11] on di-copper (I) - ligands such as **1** we investigated the effects of substituent and types of acene rings on the calculated *static* molecular first hyperpolarizabilities. We focus here on three points in regards to ligand **1**. 1) The UV-Vis spectra and nature of the first 30 excited states are calculated by vertical excitation TD-DFT in order to ascertain the number and character of the excited states nearby 400 and 532nm. 2) The calculated static and frequency dependent molecular hyperpolarizabity elements (800 and 1064nm) are compared with the experimental HRS response. 3) The total energies of the C_2 (Fig. S7)[S12] and C_i configurations (Fig. S8) are calculated to explore relative stabilities in solution.

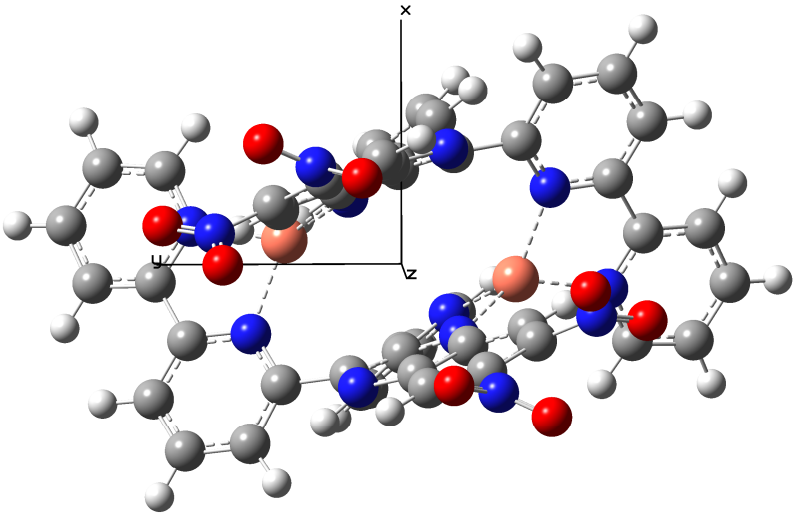

Figure S7. Results for the geometry optimization of the C_2 configuration of **1** using the PBE0/6-31+G(d)/IEPCM=acetontrile theoretical method. Dipole vector and principal axis of C_2 symmetry lie along *z*; bipyridinyl ligands lie nearly within the *xy* plane; and the pyridinyl and the projections of the diNO_2-quinoxalinyl ligands lie nearly within the *yz* plane.

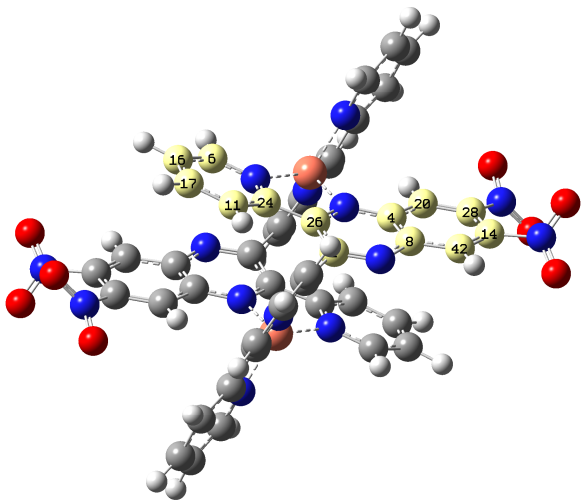

Figure S8. Results for the geometry optimization of the C_i configuration of **1** using the same theoretical method as for the C_2 configuration above. The C atoms of the top pyridinyl and diNO_2-quinoxalinyl ligand systems are coloured yellow and the numbers of the whole system are placed on the C atoms for clarity of display. The bipyridinyl ligands lie in a plane perpendicular to the page.

We continue here with the PBE0 DFT hybrid functional,[S13, S14] a solvent polarizable continuum model with the integral equation formalism variant (IEF)PCM[S15-S17] with acetonitrile ($\varepsilon = 35.688$), methanol ($\varepsilon = 32.613$) and ethanol ($\varepsilon = 24.852$), and a "general" basis set that focused on properties within the ligand regions. This basis set includes the SDD double zeta plus Stuttgart/Dresden effective core potential ECP on Cu,[S18] the 6-31+G(d) on the N,[S19, S20] the 6-31G on C, and O, and the 3-21G on the H atoms.[S21] Then some of the results for this "ligand centered" general basis set are compared to those with a 6-31+G(d) basis set *for all atoms*. This includes a second set of *d* functions, *f* functions, and diffuse functions on the Cu atoms as well as polarization and diffuse functions on the other (non H) atoms.

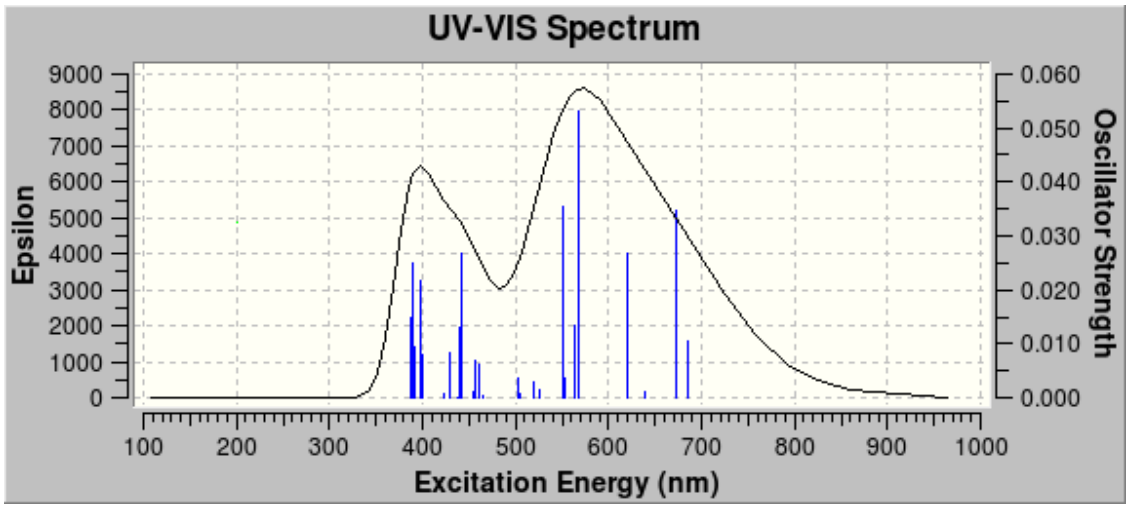

Figure S9. Calculated UV-Vis spectrum for the first 30 states in the C_2 structure using the PBE0/6-31+G(d)/IEPCM=acetonitrile theoretical method. Peak half-widths at half height: 0.20 eV. Oscillator strength in atomic units. Epsilon, molar absorption coefficient, in $mol^{-1}dm^3cm^{-1}$.

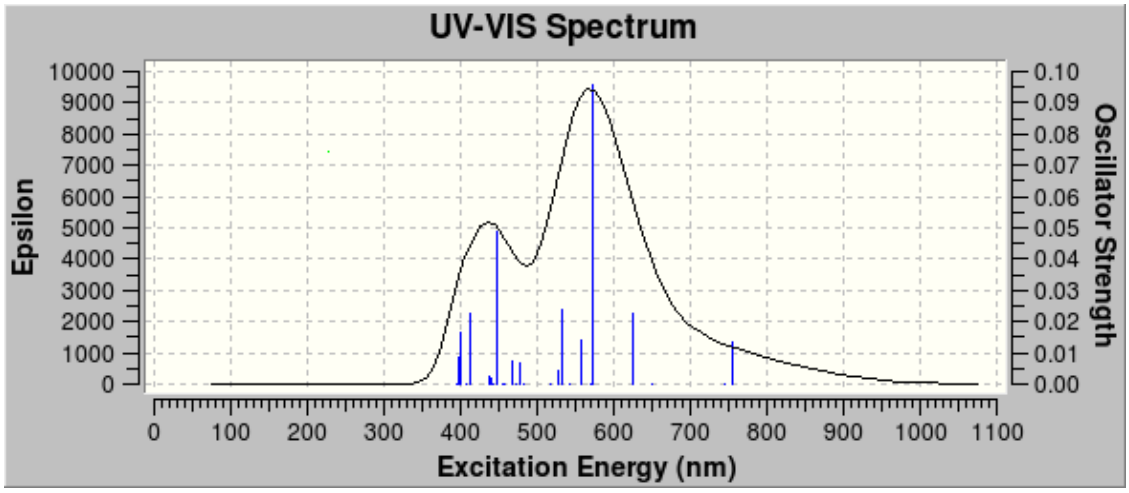

Figure S10. Calculated UV-Vis spectrum for the first 30 states in the C_i structure using the same theoretical method as for the C_2 structure above. Peak half-widths at half height: 0.20 eV. Oscillator strength in atomic units. Epsilon, molar absorption coefficient, in $mol^{-1}dm^3cm^{-1}$.

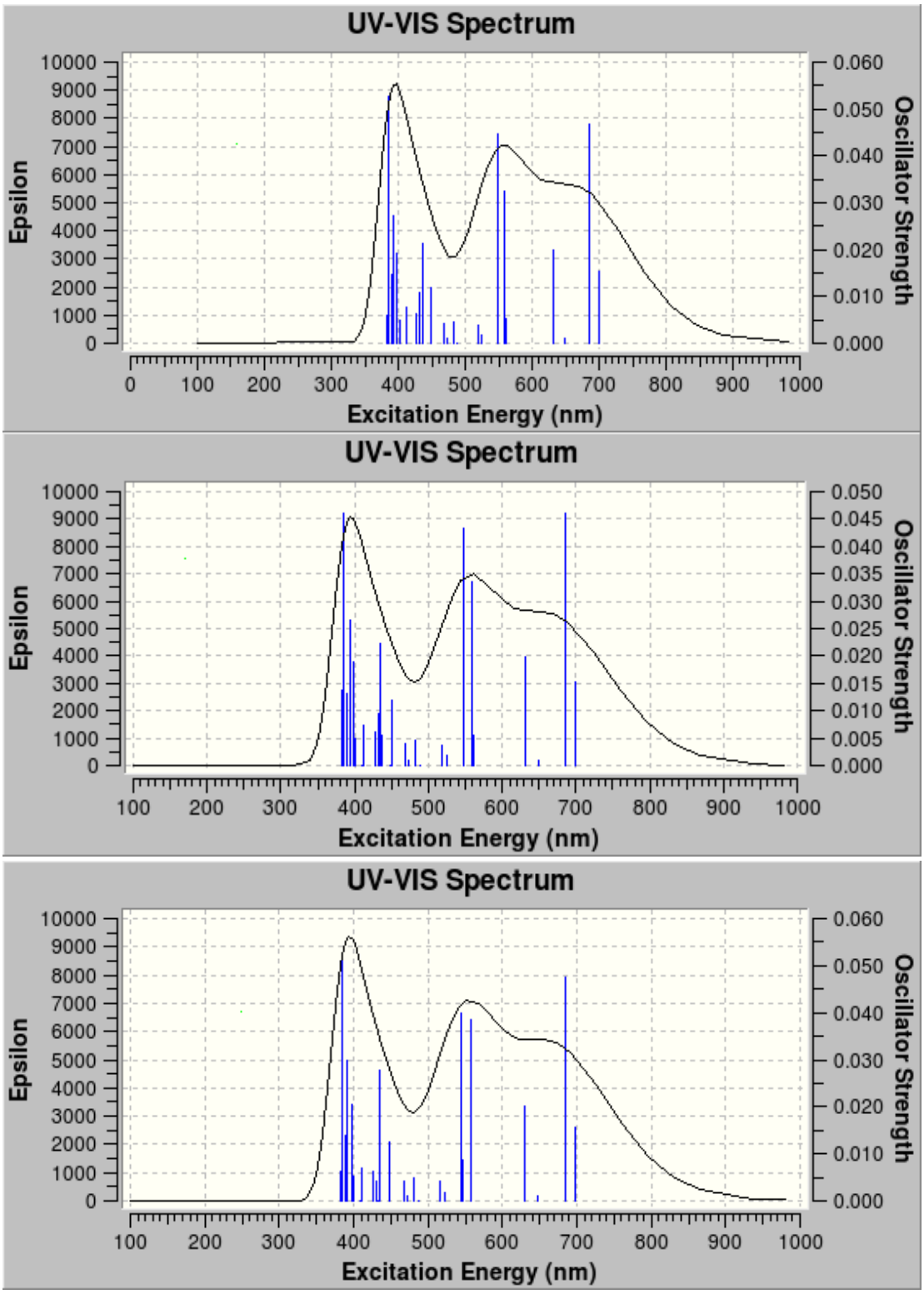

Figure S11. Calculated UV-Vis spectrum for the first 30 states in the C_2 structure using the general basis set, PBE0, and IEPCM with (top) acetonitrile, (center) methanol, (bottom) ethanol solvent parameters. Peak half-widths at half height: 0.20 eV. Oscillator strength in atomic units. Epsilon, molar absorption coefficient, in $mol^{-1}dm^3cm^{-1}$.

All calculations reported here were carried out using the default parameters in the

Gaussian09.A02 (G09) series of programs.[S22] The geometry of the complex was optimized for each choice of basis set and solvent. Due to the size of the complex the nature of the stationary points could not be checked but the framework of the complex was consistent with that calculated for complexes with smaller acene "decks" in our previous theoretical work.[S11] Also the positions of the NO_2 substituents were consistent with normal minima for functional groups (no 90° angles, etc.) and crystallographic results in this study.

The calculated UV-Vis spectrum for the first 30 excited states are given in Fig. S9 for the C_2 configuration and in Fig. S10 for C_i, (solvent = acetonitrile, 6-31+G(d) basis set). Due to the inversion symmetry in the C_i configuration only the 15 A_u states show absorbance. These are red-shifted in relation to the A and B states in C_2. Inspection of Fig. S9 shows a cluster of states between 390 and 400nm and very few between 400 to 440nm. This aspect is preserved with a change to the general basis set and the use of three solvents, Fig. S11. The calculated spectrum for ethanol in Fig. S11 (bottom) can be compared with the experimental in Fig. S4. The band at 400nm is at the start of the π inter-ligand charge transfer ILCT absorptions in all cases, while those at 440nm and above are metal- ligand charge transfer MLCT.

As is well known and much cited,[S23-S25] the molecular first hyperpolarizability (β) appears as the third rank tensor in the first nonlinear term that arises in the dependence of the induced molecular dipole moment (μ) on the applied field F experienced by the molecule. The second partial derivative of the polarization with respect to the field (evaluated at zero field) gives the first hyperpolarizability. An analogous formulation for the coefficient can be obtained from the molecular energy expansion with respect to the field. The static frequency and first hyperpolarizabilities were calculated using analytically calculated third derivatives within the coupled perturbed Kohn-Sham approach (CP-KS) rather than by the numerical finite field[S26, S27] or the perturbative Sum-over-States (SOS) methods.[S28] The β reported here are the results of a Taylor series expansion (T in the formalism of Ref. S29). The conversion factors from equivalent atomic units are μ: (1 au = 2.541746 Debye = 2.541746×10^{-18} esu×cm) and β: (1 au = 8.6392×10^{-33} esu×cm^{-5} = 3.206361×10^{-53} C^3 m^3 J^{-2}).

In Tables S1a and S2a, the non-zero molecular first hyperpolarizability components β_{ijk} are reported in (10^{-30}) esu and atomic units (au), respectively. Reports in the literature use one or the other unit; both are given here for comparison. The β_{zzz} component reflects the term along the C_2 axis which contains the dipole moment vector centered through this "3D" molecule (Fig. S7). The static (0;0,0), the (0;-ω,ω), and the (-2ω;ω,ω) (800 and 1064nm) terms were used to calculate the "laboratory frame" HRS values according to the summations given by Bersohn *et al.*,[S29] and the recapitulations of the summations given by Champagne *et al.*[S30] Equations S1 and S2 give only those elements of the summations needed with C_2 symmetry to calculate the orientational averages of the β tensor. The square root of their sum gives the total HRS response, β HRS, Equations S3 and S4. Of the 27 elements of the second-rank tensor, β_{ijk} there are a maximum of 18 that are unique since $\beta_{ijk} = \beta_{ikj}$. For structures of C_2 symmetry with the molecular dipole and principal axis aligned in the *z* direction, these reduce to 8 non-zero elements, β_{zzz}, β_{xxz}, β_{zxx}, β_{yyz}, β_{zyy}, β_{xzy}, β_{yxz}, and β_{zyx}.

$$
\begin{aligned}
\langle\beta^2_{ZZZ}\,\mathrm{HRS}\rangle = {} & (1/7)\beta_{zzz}^2 + (4/35)\,\beta_{zzz}(\beta_{xxz}+\beta_{yyz}) + (4/35)\,(\beta_{xxz}^2+\beta_{yyz}^2) \\
& + (2/35)\,\beta_{zzz}(\beta_{zxx}+\beta_{zyy}) + (1/35)\,(\beta_{zxx}^2+\beta_{zyy}^2) \\
& + (4/35)\,(\beta_{zxx}\beta_{xxz}+\beta_{zyy}\beta_{yyz}) + (4/105)\,(\beta_{xxz}\beta_{zyy}+\beta_{yyz}\beta_{zxx}) \\
& + (2/105)\,\beta_{zyy}\beta_{zxx} + (8/105)\,\beta_{xxz}\beta_{yyz} \\
& + (8/105)\,(\beta_{zyx}\beta_{yxz}+\beta_{zyx}\beta_{xzy}+\beta_{yxz}\beta_{xzy}) + (4/105)\,(\beta_{xzy}^2+\beta_{yxz}^2+\beta_{zyx}^2) \quad \text{(S1)} \\
\langle\beta^2_{XZZ}\,\mathrm{HRS}\rangle = {} & (1/35)\beta_{zzz}^2 - (2/35)\,\beta_{zzz}(\beta_{xxz}+\beta_{yyz}) + (8/105)\,(\beta_{xxz}^2+\beta_{yyz}^2)
\end{aligned}
$$

$$+ (4/105)\, \beta_{zzz}(\beta_{zxx} + \beta_{zyy}) + (3/35)\, (\beta_{zxx}^2 + \beta_{zyy}^2)$$
$$- (2/35)\, (\beta_{zxx}\beta_{xxz} + \beta_{zyy}\beta_{yyz}) - (2/105)\, (\beta_{xxz}\beta_{zyy} + \beta_{yyz}\beta_{zxx})$$
$$+ (2/35)\, \beta_{zyy}\beta_{zxx} - (4/105)\, \beta_{xxz}\beta_{yyz}$$
$$- (4/105)\, (\beta_{zyx}\beta_{yxz} + \beta_{zyx}\beta_{xzy} + \beta_{yxz}\beta_{xzy}) + (4/35)\, (\beta_{xzy}^2 + \beta_{yxz}^2 + \beta_{zyx}^2) \qquad \text{(S2)}$$

$$\langle\beta^2_{TOTAL}\, HRS\rangle = \langle\beta^2_{ZZZ}\, HRS\rangle + \langle\beta^2_{XZZ}\, HRS\rangle \qquad \text{(S3)}$$

$$\beta\ HRS = (\langle\beta^2_{TOTAL}\, HRS\rangle)^{1/2} \qquad \text{(S4)}$$

The results for the calculated HRS responses are given in Tables S1b and S2b. At the static, 0nm, values "Kleinman symmetry conditions" apply and the three β_{zii}, β_{iiz}, β_{izi} components are equal as well as the three pairs of β_{ijz} components. However, in general at any particular incident wavelength > 0nm, $\beta_{iiz} = \beta_{izi} \neq \beta_{zii}$ and $\beta_{ijk} = \beta_{ikj}$ but $\beta_{xij} \neq \beta_{yij} \neq \beta_{zij}$. in the (-2ω;ω,ω) convention of Bersohn *et al.*[S29] The change in the calculated values of β from the static values and the extent of the breaking of "Kleinman symmetry" $\beta_{iiz} \neq \beta_{zii}$ and $\beta_{xij} \neq \beta_{yij}$ might be used as an indication of resonance at the frequency doubling. It is to be noted that the Gaussian09 program uses the convention for dc-Pockels β(−ω,ω;0), where $\beta_{iiz} \neq \beta_{izi} = \beta_{zii}$, not that of Bersohn for Second-Harmonic Generation SHG, β(-2ω;ω,ω). For example, the 18 unique values of the 27 tensor elements β_{ijk} are listed in Gaussian09 over three "K blocks 1,2,3" each containing the three diagonal and three lower left values of the nine values, while not listing the other three duplicate, off diagonal values. Taking Block 1, where k = X, and the i,j value listed for the off diagonal z,x equals the (unlisted) value for x,z. Thus z,x,X = x,z,X, $\beta_{zxx} = \beta_{xzx}$. but in Block 3 where k = Z, there is only one value when i,j = x,x, xxZ or β_{xxz}. In equations S1 and S2, Gaussian09 off diagonal values of β_{zii} (=β_{izi}) (ω,ω;-2ω) were used for the (-2ω,ω,ω) Bersohn β_{iiz} (=β_{izi}), and Gaussian09 single, diagonal values of β_{iiz} were used for the single Bersohn value for β_{zii}. A similar transposition was effected for the β_{ijk} values.

In Table S1b, with the general and 6-31+G(d) basis sets $\langle\beta^2_{XZZ}\, HRS\rangle$ = 4000 to 5000 10^{-30} esu and $\langle\beta^2_{XZZ}\, HRS\rangle$ = 500 to 700 10^{-30} esu, with the total $\langle\beta^2_{TOTAL}\, HRS\rangle$ = 5000 to 5800 10^{-30} esu at 0 and 1064nm. Corresponding values are 80 to 90% less with the 6-31+G(d) basis set than the general. The major discrepancy in basis set results are the ratios of $\langle\beta_{XZZ}^2{}_{HRS}\rangle$ to $\langle\beta_{ZZZ}^2{}_{HRS}\rangle$ at 800nm, (-2ω;ω,ω) with the 6-31+G(d) set giving a higher value for the "off-diagonal" component $\langle\beta_{XZZ}^2{}_{HRS}\rangle$. The total responses, however, are nearly equivalent. Inspection of Fig. S9 shows no significant states between 500 and 550nm for the C_2 configuration using either basis set. Incident light at 1064nm should display little resonance around 532nm as seen with the difference between the β_{iiz} and β_{zii} values and closeness of each of these values to the corresponding values at 0nm.

The total HRS results for both basis sets are *ca.* 320 (10^{-30}) esu a factor of 3 higher than the static results, but still an order of magnitude less than experiment. Although Kleinman symmetry is broken, $\beta_{iiz} \neq \beta_{zii}$ and $\beta_{ijz} \neq \beta_{jiz} \neq \beta_{zij}$. at (-2ω,ω,ω) 800nm, the total HRS response is only a factor of three higher than *static* values. This small factor, combined with a large density of ILCT states starting below 400nm indicate that the amount of resonance at 400nm is not a major contributor to the (calculated) HRS response. Resonance enhancement of the zero-frequency β_0 can be estimated using Oudar and Chemla's{S31} two-level model where the difference in energy between the ground and the CT state is 1.8068 eV and the energy of the incident photon at 800 nm is 1.5498 eV. The resonance enhanced β_λ is a factor of 1.95 times β_0.

A change in solvent from MeCN (ε = 35.688) to MeOH (ε = 32.613), which was used in the experimental HRS, is not expected to change the calculated HRS response significantly, given that results are similar for the 1) calculated states nearby 400nm and 2) calculated molecular β elements for (0;-ω,ω) at 800nm (Tables S1a and b).

Finally, using the 6-31+G(d) basis set the energies of the geometry optimized C_2 and C_i configurations are -6413.130837 and -6413.126060 a.u., respectively The C_2 is thus lower by 3.00 kcal/mol (12.4 kJ/mol).

Table S1a. Calculated molecular hyperpolarizabilities (10^{-30}) esu) with the general and 6-31+G(d) basis sets. All values are for (0;-ω,ω), except where noted -2ω for (-2ω;ω,ω). Solvent is MeCN, except where noted MeOH.

Conditions, esu	βxxz	βzxx	βzyx	βyxz	βxzy	βyyz	βzyy	βzzz
General, **0nm**	26.56	26.56	-7.57	-7.57	-7.57	65.10	65.10	112.75
800nm	74.09	86.59	-63.46	-29.92	-24.87	203.74	333.41	246.88
800nm MeOH	72.6	84.8	-61.7	-29.2	-24.1	199.9	326.5	241.6
800nm (-2ω)	-7.67	220.45	142.60	67.22	-108.12	-114.30	242.45	581.39
1064nm	26.38	29.82	-9.62	-5.86	-5.69	68.53	86.84	97.55
1064nm (-2ω)	-63.26	-39.05	7.57	94.98	117.35	-184.70	-91.39	36.89
631+G(d), **0nm**	26.08	26.08	-11.06	-11.06	-11.06	60.09	60.09	103.42
800nm	67.22	93.71	-61.68	-31.23	-39.33	128.53	214.90	187.47
800nm (-2ω)	-44.35	125.33	154.85	234.98	-142.55	-496.95	206.55	484.81
1064nm	25.77	31.54	-13.30	-8.73	-10.44	58.08	73.39	91.17
1064nm (-2ω)	-73.53	-38.38	9.58	89.10	108.45	-133.61	-35.84	44.52

Table S1b. Orientational averages of the macroscopic β^2 tensor and their sum (Equation S3) $(10^{-30}\text{esu})^2$, and total HRS response $\beta_{HRS}(10^{-30})$ esu (Equation S4). All values are for (0;-ω,ω), except where noted -2ω for (-2ω,ω,ω). Solvent is MeCN, except where noted MeOH.

Conditions, esu	$<\beta_{ZZZ}^2{}_{HRS}>$	$<\beta_{XZZ}^2{}_{HRS}>$	$<\beta_{TOT}^2{}_{HRS}>$
General, **0nm**	5.17E+03	6.64E+02	5.84E+03
800nm	4.36E+04	1.20E+04	5.56E+04
800nm MeOH	4.18E+04	1.15E+04	5.33E+04
800nm (-2ω)	5.72E+04	4.41E+04	1.01E+05
1064nm	5.06E+03	9.34E+02	6.00E+03
1064nm (-2ω)	9.02E+03	4.66E+03	1.37E+04
631+G(d), **0nm**	4.47E+03	5.84E+02	5.05E+03
800nm	2.31E+04	6.31E+03	2.94E+04
800nm (-2ω)	3.23E+04	7.21E+04	1.04E+05
1064nm	4.17E+03	7.62E+02	4.93E+03
1064nm (-2ω)	5.35E+03	3.41E+03	8.76E+03

Table S2a. Calculated molecular hyperpolarizabilities (a.u.). All values are for (0;-ω,ω), except where noted -2ω for (-2ω;ω,ω). Solvent is MeCN.

Conditions, esu	βxxz	βzxx	βzyx	βyxz	βxzy	βyyz	βzyy	βzzz
Gen, **0nm**	3074	3074	-876	-876	-876	7535	7535	13051
800nm	8576	10023	-7346	-3463	-2879	23583	38593	28577
800nm (-2ω)	-888	25518	16506	7781	-12515	-13231	28064	67297
1064nm	3054	3452	-1113	-678	-659	7933	10052	11291
1064nm (-2ω)	-7322	-4520	876	10994	13583	-21379	-10578	4270
631+G(d), **0nm**	3019	3019	-1280	-1280	-1280	6956	6956	11971
800nm	7781	10847	-7140	-3615	-4553	14877	24875	21700
800nm (-2ω)	-5133	14507	17924	27199	-16500	-57523	23908	56118
1064nm	2983	3651	-1540	-1010	-1208	6723	8495	10553
1064nm (-2ω)	-8511	-4443	1109	10314	12553	-15465	-4148	5153

Table S2b. Orientational averages of the macroscopic β^2 tensor and their sum (Equation S3)(a.u.)^2, and total HRS response β_{HRS}(au) (Equation S4). All values are for (0;-ω,ω), except where noted -2ω for (-2ω,ω,ω). Solvent is MeCN.

Conditions, au	$<\beta^2_{ZZZ\ HRS}>$	$<\beta^2_{XZZ\ HRS}>$	$<\beta^2_{TOT\ HRS}>$
Gen, **0nm**	693.3E+5	890.1E+4	782.3E+5
800nm	583.8E+6	161.0E+6	744.8E+6
800nm (-2ω)	766.6E+6	590.3E+6	135.7E+7
1064nm	678.5E+5	125.1E+5	803.7E+5
1064nm (-2ω)	120.8E+6	624.4E+5	183.3E+6
631+G(d), **0nm**	598.9E+5	781.8E+4	677.1E+5
800nm	309.4E+6	846.0E+5	394.0E+6
800nm (-2ω)	432.9E+6	966.0E+6	139.9E+7
1064nm	558.9E+5	102.1E+5	661.1E+5
1064nm (-2ω)	717.1E+5	456.8E+5	117.4E+6

S5 References

S1. F. R. Heirtzler, *Synlett*, 1999, 1203-1206.
S2. G. W. Cheeseman, *J. Chem. Soc.*, 1962, 1170-1176.
S3. H. Wang, T. Troxler, A.-G. Yeh and H.-L. Dai, *Langmuir*, 2000, 16, 2475-2481.
S4. S.-H. Jen and H.-L. Dai, *J. Phys. Chem. B*, 2006, 110, 23000-23003.
S5. S.-H. Jen, G. Gonella and H.-L. Dai, *J. Phys. Chem. A*, 2009, 113, 4758-4762.
S6. T. Verbiest, K. Clays, C. Samyn, J. Wolff, D. Reinhoudt and A. Persoons, *J. Am. Chem. Soc.*, 1994, 116, 9320-9323.
S7. I. Asselberghs, J. Pérez-Moreno and K. Clays, in *Non-Linear Optical Properties of Matter*, eds. M. G. Papadopoulos, A. J. Sadlej and J. Leszczynski, Springer Netherlands, 2006, vol. 1, pp. 419-459.
S8. K. Clays and A. Persoons, *Phys. Rev. Lett.*, 1991, 66, 2980.
S9. T. Verbiest, K. Clays, A. Persoons, F. Meyers and J. L. Bredas, *Opt. Lett.*, 1993, 18, 525-527.
S10. G. Revillod, J. Duboisset, I. Russier-Antoine, E. Benichou, G. Bachelier, C. Jonin and P.-F. Brevet, *J. Phys. Chem. C*, 2008, 112, 2716-2723.
S11. L. A. Burke and F. Heirtzler, *Int. J. Quantum Chem.*, 2010, 110, 3061-3071.
S12. The images for Fig. S7-S11 were generated by the GaussView program, R. K. Dennington, T.; Millam, J., Semichem Inc. , *GaussView Version 5*, Shawnee Mission, KS 2009.
S13. C. Adamo and V. Barone, *J. Chem. Phys.*, 1999, 110, 6158-6170.
S14. The accuracy of the PBE0 functional within vertical TD-DFT calculations has been "benchmarked" in D. Jacquemin, V. Wathelet, E. A. Perpete and C. Adamo, *J. Chem. Theory Comput.*, 2009, 5, 2420-2435.
S15. V. Barone, M. Cossi and J. Tomasi, *J. Comput. Chem.*, 1998, 19, 404-417.
S16. R. Cammi, M. Cossi, B. Mennucci and J. Tomasi, *J. Mol. Struct.*, 1997, 437, 567-575.
S17. E. Cances, B. Mennucci and J. Tomasi, *J. Chem. Phys.*, 1997, 107, 3032-3041.
S18. D. Andrae, U. Haussermann, M. Dolg, H. Stoll and H. Preuss, *Theor. Chim. Acta*, 1990, 77, 123-141.
S19. J. Chandrasekhar, J. G. Andrade and P. V. Schleyer, *J. Am. Chem. Soc.*, 1981, 103, 5609-5612.
S20. T. Clark, J. Chandrasekhar, G. W. Spitznagel and P. V. Schleyer, *J. Comput. Chem.*, 1983, 4, 294-301.
S21. M. M. Francl, W. J. Pietro, W. J. Hehre, J. S. Binkley, M. S. Gordon, D. J. Defrees and J. A. Pople, *J. Chem. Phys.*, 1982, 77, 3654-3665 and references therein.
S22. M. J. Frisch, G. W. Trucks, H. B. Schlegel, G. E. Scuseria, M. A. Robb, J. R. Cheeseman, G. Scalmani, V. Barone, B. Mennucci, G. A. Petersson, H. Nakatsuji, M. Caricato, X. Li, H. P. Hratchian, A. F. Izmaylov, J. Bloino, G. Zheng, J. L. Sonnenberg, M. Hada, M. Ehara, K. Toyota, R. Fukuda, J. Hasegawa, M. Ishida, T. Nakajima, Y. Honda, O. Kitao, H. Nakai, T. Vreven, J. A. Montgomery, J. E. Peralta, F. Ogliaro, M. Bearpark, J. J. Heyd, E. Brothers, K. N. Kudin, V. N. Staroverov, R. Kobayashi, J. Normand, K. Raghavachari, A. Rendell, J. C. Burant, S. S. Iyengar, J. Tomasi, M. Cossi, N. Rega, J. M. Millam, M. Klene, J. E. Knox, J. B. Cross, V. Bakken, C. Adamo, J. Jaramillo, R. Gomperts, R. E. Stratmann, O. Yazyev, A. J. Austin, R. Cammi, C. Pomelli, J. W. Ochterski, R. L. Martin, K. Morokuma, V. G. Zakrzewski, G. A. Voth, P. Salvador, J. J. Dannenberg, S. Dapprich, A. D. Daniels, Farkas, J. B. Foresman, J. V. Ortiz, J. Cioslowski and D. J. Fox, *Gaussian 09, Revision A.02*, Wallingford CT, 2009.

S23. B. J. Coe, S. P. Foxon, E. C. Harper, M. Helliwell, J. Raftery, C. A. Swanson, B. S. Brunschwig, K. Clays, E. Franz, J. Garin, J. Orduna, P. N. Horton and M. B. Hursthouse, *J. Am. Chem. Soc.*, 2010, 132, 1706-1723.
S24. J. Zyss, *Molecular nonlinear optics: materials, physics, and devices*, Academic Press, 1994.
S25. T. J. Marks and M. A. Ratner, *Angew. Chem. Int. Edit.*, 1995, 34, 155-173.
S26. H. D. Cohen and C. C. Roothaan, *J. Chem. Phys.*, 1965, 43, S034-+.
S27. H. A. Kurtz, J. J. P. Stewart and K. M. Dieter, *J. Comput. Chem.*, 1990, 11, 82-87.
S28. B. J. Orr and J. F. Ward, *Mol. Phys.*, 1971, 20, 513-&.
S29. R. Bersohn, Y. H. Pao and H. L. Frisch, *J. Chem. Phys.*, 1966, 45, 3184-&.
S30. S. N. Labidi, M. B. Kanoun, M. De Wergifosse and B. Champagne, *Int. J. Quantum Chem.*, 2011, 111, 1583-1595.
S31. J. L. Oudar and D. S. Chemla, *J. Chem. Phys.*, 1977, 66, 2664–2668.